Water Science & Technology

Electrochemical degradation of ciprofloxacin through a DoE-driven optimization in a filter-press type reactor under batch recirculation mode

Ever Peralta-Reyes [iD] [a], Alejandro Regalado-Méndez [iD] [a,*], Alexis A. Chimeo-Sánchez[a], Edson E. Robles-Gómez[a] and Reyna Natividad[b]

[a] Investigation Laboratories, Universidad del Mar, Puerto Ángel, Oaxaca 70902, México
[b] Chemical Engineering Laboratory, Centro Conjunto de Investigación en Química Sustentable, UAEMex-UNAM, Universidad Autónoma del Estado de México, Estado de México, Toluca 50200, México
*Corresponding author. E-mail: alejandro.regalado33@gmail.com

[iD] EP, 0000-0003-0018-6549; AR, 0000-0002-5270-745X

ABSTRACT

In this work, the electrochemical degradation of ciprofloxacin (CIP) was studied in a filter-press-type reactor without division in a batch recirculation manner. For this purpose, two boron-doped diamond (BDD) electrodes (as cathode and anode) were employed. Also, the optimal operating conditions were found by response surface methodology (RSM) following a central composite face-centered design with three factors, namely current intensity (i), initial pH (pH_0), and initial concentration ($[C]_0$) with two responses, namely remotion efficiency (η) and operating cost. Optimal operating conditions were $i = 3$ A, $pH_0 = 8.49$, and $[C]_0 = 33.26$ mg L^{-1} within an electrolysis time of 5 h, leading to a maximum removal efficiency of 93.49% with a minimum operating cost of \$0.013 USD L^{-1}. Also, a TOC analysis shows an 80% of mineralization extent with an energy consumption of 5.11 kWh g^{-1} TOC. Furthermore, the CIP degradation progress was followed by mass spectrometry (LC/MS) and a degradation pathway is proposed.

Key words: BDD electrodes, central composite face-centered design, ciprofloxacin, degradation pathway, DoE-driven optimization

HIGHLIGHTS

- Ciprofloxacin has been removed efficiently in a flow-by reactor equipped with two BDD electrodes.
- Optimal operating conditions were $pH_0 = 8.49$, $i = 3$ A, and $[C]_0 = 33.26$ mg L^{-1}.
- Mineralization efficiency and extent of electrochemical combustion at optimal operating conditions were 80% and 0.85.
- Three pathway reactions for the electrochemical degradation of CIP were described.
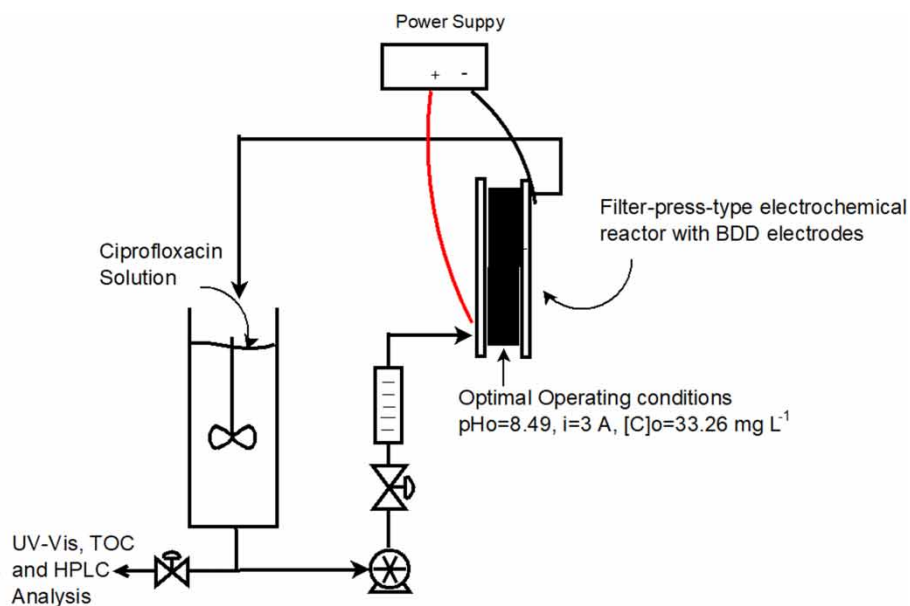
GRAPHICAL ABSTRACT
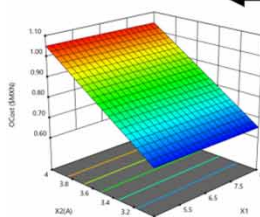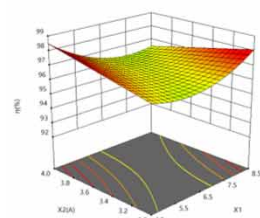
1. INTRODUCTION

In recent years, a special concern has been raised with the presence of emerging pollutant compounds (EC) in water bodies (e.g., rivers, lakes, and oceans) (Ojo *et al.* 2022) and soils (e.g., farming, cattle raising, and highway) because these can cause human health and environmental issues. EC, also known as micropollutants, can be either synthetic or from a natural origin (Khan *et al.* 2020; Arman *et al.* 2021; Firdaus *et al.* 2021). Common EC are personal cleaning products and drugs (e.g., hormones, antibiotics, analgesics, antidepressants, pesticides, among others) (Goswami *et al.* 2022). Although drugs are essential to human and animal welfare, they are harmful to the environment since they are introduced into water bodies (e.g., wastewater) (Rivera-Utrilla *et al.* 2013) by excretion and urine through sewage, slurry, and rainfall. Among the EC are fluoroquinolones such as ciprofloxacin (CIP), which is the most used antibiotic for many diseases (e.g., respiratory and bacterial) (Ashfaq *et al.* 2016). Also, CIP was employed during the COVID-19 pandemic as a complementary treatment (Cappelli *et al.* 2022). However, intensive use is dangerous to the environment since CIP is not completely metabolized by the human body and animals causing accumulation in water and promoting resistance to antibiotics resulting in risks to human health (Ahmadzadeh *et al.* 2017; Kim *et al.* 2020). In this context, the presence of EC (such as CIP) in wastewater has motivated the development of technologies to eliminate these since conventional wastewater treatments do not exhibit a high degradation efficiency. The advanced oxidation processes (AOPs, e.g., anodic oxidation (AO), electro-Fenton, photo-electro-Fenton, solar-photo-electro-Fenton, among others (Moreira *et al.* 2017)), emerge as an efficient technique to remove EC. AOPs are based on the generation of hydroxyl radicals (OH$^{\cdot}$). In this sense, the AO becomes a green, efficient energetic, versatile, profitable, easily automatized, and promising technology (Martín de Vidales *et al.* 2020; Firdaus *et al.* 2021) for wastewater treatment.

AO has the advantage of producing hydroxyl radicals without the addition of chemicals (e.g., hydrogen peroxide and FeSO$_4$, like in the Fenton process) since the water is oxidized in the anode surface according to the following equation (Chaplin 2014),

$$H_2O \rightarrow OH^{\cdot} + H^+ + e^- \tag{1}$$

OH$^{\cdot}$ is capable of oxidizing and mineralizing organic compounds such as EC until carbon dioxide (CO$_2$), ions, and water. Also, the amount of OH$^{\cdot}$ is dependent on the anode material because the overpotential of the oxygen evolution reaction is different for each anode material. In this sense, the boron-doped diamond (BDD) electrode exhibits a high overpotential of

the oxygen evolution reaction. Therefore, the BDD anode is widely employed for the generation of OH$^{\cdot}$ (Auguste & Ouattara 2021).

Table 1 presents a summary of the literature related to the electrochemical degradation of CIP by using different anode materials, different reactor configurations, and different reaction environments. Although the literature review reveals high removal efficiencies of CIP, the treatment volume employed in many cases is very small, and the operating cost for all studies is not reported. In addition, it is observed in Table 1 that the optimization of the electrochemical degradation of CIP has not been yet intensively performed.

Table 1 | Degradation of CIP at different environment reaction conditions

Operating conditions		Electrodes	V (L)	Main results			Ref.
Optimized	Not optimized			ED (%)	TOC (%)	DQO (%)	
Batch reactor, pH$_0$ = 9, j = 17 mA cm^{-2}, [Na$_2$SO$_4$] = 1.5 mg L^{-1}, and t = 5 h		Ti/SnO$_2$-Sb$_2$O$_5$, Ti/RuO$_2$-Ti	0.2			89.5	Firdaus et al. (2021)
	Flow reactor, Q = 2.5 L min^{-1}, pH$_0$ = 10, j = 30 mA cm^{-2}, [C]$_0$ = 50 mg L^{-1}, [Na$_2$SO$_4$] = 0.1 mol L^{-1}, and t = 10 h	BDD-stainless steel 304	0.5	100	100		Wachter et al. (2019a)
	Flow reactor, Q = 6.5 L min^{-1}, pH$_0$ = 10, j = 30 mA cm^{-2}, [C]$_0$ = 50 mg L^{-1}, [Na$_2$SO$_4$] = 0.1 mol L^{-1}, and t = 5 h	Ni-TiPt/β-PBO$_2$ – Ni BDD-Stainless steel 304	0.5	100	75		Wachter et al. (2019b)
	Flow reactor, Q = 7 L min^{-1}, j = 10 mA cm^{-2} [C]$_0$ = 100 mg L^{-1}, [NaCl] = 0.1 mol L^{-1}, and t = 8 h	BDD-Stainless steel 304	1	100	80		Carneiro et al. (2020)
	Flow reactor, Q = 0.4 L min^{-1}, j = 30 mA cm^{-2}, pH = 7, [C]$_0$ = 10 mg L^{-1}, and t = 0.33 h	BDD-Ti	0.3	100			Li et al. (2019)
	Batch reactor, j = 50 mA cm^{-2}, pH$_0$ = 2.5, [C]$_0$ = 30 mg L^{-1}, [K$_2$SO$_4$] = 0.1 mol L^{-1}, and t = 1.5 h	Ti–Pt-EDG	0.25	99.3	25.3		Lima et al. (2020)
	Batch reactor, j = 30 mA cm^{-2}, pH$_0$ = 5.4, [C]$_0$ = 50 mg L^{-1}, [Na$_2$SO$_4$] = 0.05 mol L^{-1}, and t = 2 h	SnO$_2$-Sb/Ti-Ti	0.25	99.5	70		Wang et al. (2016)
	Batch reactor, j = 20 mA cm^{-2}, pH$_0$ = 3, [C]$_0$ = 30 mg L^{-1}, [Na$_2$SO$_4$] = 25 g L^{-1}, and t = 1.5 h	Doped Sb SnO$_2$-Stainless steel	0.05	100	93		Mu et al. (2019)
	Batch reactor, j = 40 mA cm^{-2}, pH$_0$ = 7, [C]$_0$ = 15 mg L^{-1}, Chloride medium, and t = 0.33 h	BDD (NCD)-Stainless steel	0.1	100	37.4		dos Santos et al. (2022)

(*Continued.*)

Table 1 | Continued

Operating conditions				Main results			
Optimized	Not optimized	Electrodes	V (L)	ED (%)	TOC (%)	DQO (%)	Ref.
	Real wastewater, $j = 40$ mA cm^{-2}, pH$_0 = 7$, $[C]_0 = 15$ mg L^{-1}, and $t = 1$ h	BDD (NCD)-Stainless steel	0.1	100	28.7		
	Synthetic urine, $j = 40$ mA cm^{-2}, pH$_0 = 7$, $[C]_0 = 15$ mg L^{-1}, and $t = 1$ h	BDD (NCD)-Stainless steel	0.1	90.4	32.2		
	Batch reactor, pure water, $j = 45$ mA cm^{-2}, pH$_0 = 7$, $[C]_0 = 10$ mg L^{-1}, $[Na_2SO_4] = 0.05$ M, and $t = 5$ h	BDD-Stainless steel	2.0	99.9			Montenegro-Ayo *et al.* (2023)
	Batch reactor, tap water, $[Na_2SO_4] = 0.05$ M, $[C]_0 = 10$ mg L^{-1}, $j = 45$ mA cm^{-2}, pH$_0 = 6.5$, and, $t = 5$ h	BDD-Stainless steal	2.0	95.8			
	Batch reactor, synthetic urine, $[C]_0 = 10$ mg L^{-1}, $[Na_2SO_4] = 0.05$ M, $j = 45$ mA cm^{-2}, pH$_0 = 7$, and $t = 5$ h	BDD-Stainless steel	2.0	77.2			
	Batch reactor, synthetic urine, $[C]_0 = 30$ mg L^{-1}, $[Na_2SO_4] = 0.05$ M, $j = 45$ mA cm^{-2}, pH$_0 = 7$, and $t = 5$ h	BDD-Stainless steel	2.0			94	
Batch reactor, $j = 3.5$ mA cm^{-2}, pH$_0 = 3$, $[C]_0 = 10$ mg L^{-1}, $[NaCl] = 10$ mg L^{-1}, and $t = 1.5$ h		Ti/nanoSnO$_2$MWCN-Stainless steel	0.25	89.61			Esmaelian *et al.* (2019)

Based on the above-mentioned, the objective of this work was the electrochemical degradation of CIP through a DoE-driven optimization in a filter-press-type reactor under batch recirculation mode equipped with two BDD electrodes (both as anode and cathode). For this case, a central composite face-centered experimental design was utilized with three factors namely the initial concentration of CIP ($[C]_0$), initial hydrogen potential (pH$_0$), and current intensity (i) with two response variables namely removal efficiency (η) and operating cost (*OCost*).

2. MATERIALS AND METHODS

2.1. Reagents and synthetic solution of CIP

CIP (CAS No: 85721-33-1, MW: 331.34 g mol^{-1}, grade high-performance liquid chromatography (HPLC)), Na$_2$SO$_4$, NaOH, H$_2$SO$_4$ with a purity of 98, 99, 97, and 95–98%, respectively. All chemicals were purchased from Sigma Aldrich Company.

Synthetic solutions of CIP at different initial concentrations were prepared before running each experiment with 0.15 M of Na$_2$SO$_4$ as a supporting electrolyte. Also, 2 M NaOH and H$_2$SO$_4$ solutions, respectively, were prepared to adjust the pH$_0$. It is worth mentioning that all aqueous solutions were prepared with distilled water.

2.2. Equipment

The pH was measured by using a potentiometer Hanna HI2210, and a power supply Gw instek GPR-351OHD was used to provide energy at the filter-press electrochemical reactor. The employed filter-press-type reactor was equipped with BDD electrodes that are separated 1.1 cm from each other. Also, has a reactor volume of 3.52×10^{-5} m^3, a height of 20 cm, a width of 4.8 cm, and an electro active area of 32 cm^2. In Figure 1, a schematic diagram of the filter-press-type electrochemical system
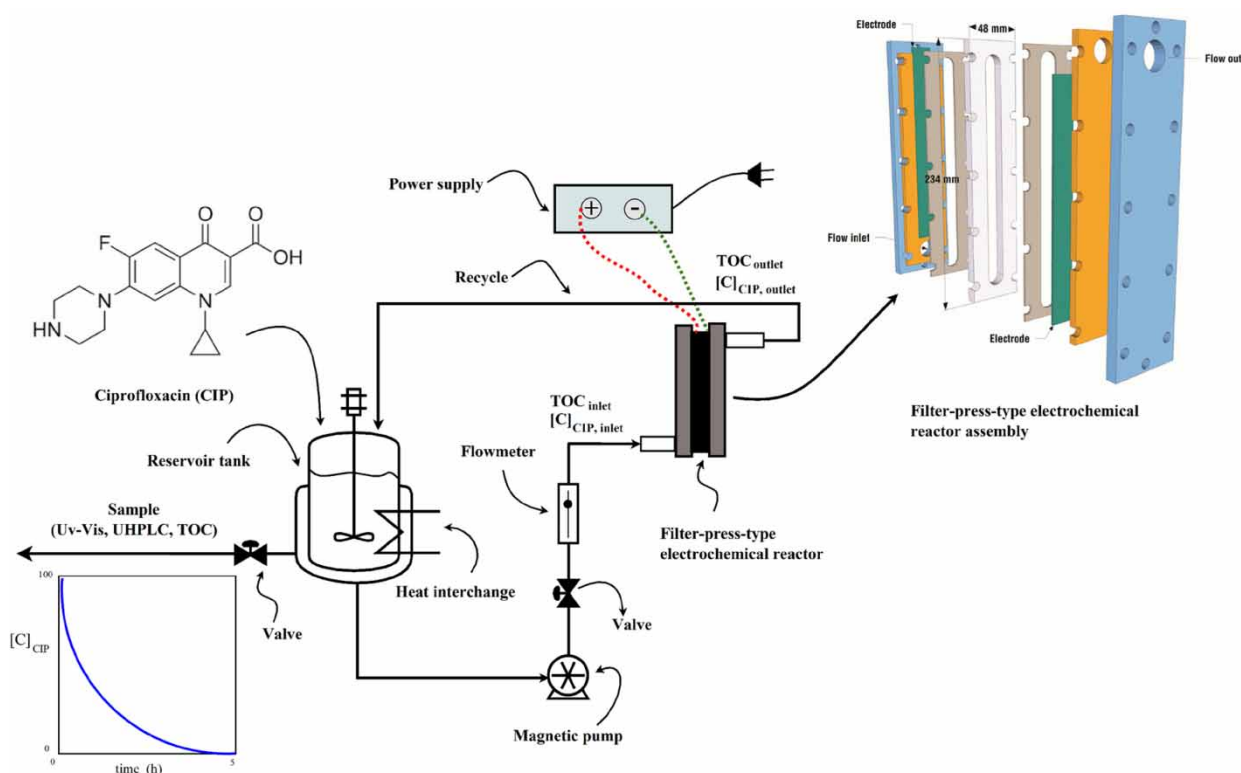
Figure 1 | Schematic diagram of the experimental set-up with a filter-press-type electrochemical reactor.

can be observed. Additionally, at the optimal operating conditions, the total organic carbon was determined by employing a TOC Analyzer Shimadzu TOC-6001. For the optimization process, the CIP was quantified by UV-Vis spectrophotometry in a UV-Vis PerkinElmer Lambda 365 spectrophotometer.

2.3. Analytical procedures

2.3.1. Removal efficiency

The removal efficiency (η) of CIP was determined based on absorbance lectures at 272 nm according to Equation (2) (Lupa *et al.* 2020). For this purpose, the absorbance of samples taken at the beginning (A_0) and the end (A_t) of each run were measured in a spectrophotometer UV-Vis Perkin Elmer Lambda 365. While the η under optimal operating conditions was computed by using Equation (3),

$$\eta(\%) = \frac{A_0 - A_t}{A_0} \times 100 \tag{2}$$

$$\eta(\%) = \frac{C_0 - C_t}{C_0} \times 100 \tag{3}$$

where C_0 is the initial concentration of CIP and C_t is the concentration of CIP at electrolysis time t (h).

2.3.2. Operating cost

The operating cost (*OCost*) was computed by the set of Equations (4)–(6) according to reference (Barrera-Díaz *et al.* 2018),

$$OCost = E \times \$kWh \tag{4}$$

$$E = P \times t \tag{5}$$

$$P = \frac{i \times \psi}{1,000} \tag{6}$$

where E is the energy (kWh), 3.07 \$MXN per kWh is the average price per kWh for commercial use in Mexico (Energy was supplied by the Mexican Company of Federal Commission of Electricity (CFE)), P is the power (kW), i is current intensity (A), ψ is the electrical potential (V).

2.3.3. Mineralization current efficiency

The mineralization current efficiency (MCE) provides a measurement of the effectiveness of the detoxification of wastewater treatment. The MCE is based on the difference between the initial and final *TOC* according to the following equation (Guinea *et al.* 2008),

$$MCE(\%) = \frac{nFV_s\Delta(TOC)_{Exp}}{4.32 \times 10^7 m \times i \times t} \tag{7}$$

where F is the Faraday constant (96,487 C mol^{-1}), V_s is the volume of treatment (L), $\Delta(TOC)_{Exp}$ is the change of experimental TOC at electrolysis time (mg L^{-1}), 4.32×10^7 mg s mol^{-1} h^{-1} is a conversion factor, m is the number of carbon atoms, and n is the number of electrons required (in this case are 94) to reach the total mineralization of CIP into CO_2 and inorganic ions as shown in the following equation

$$C_{17}H_{18}FN_3O_3 + 40H_2O \rightarrow 17CO_2 + F^- + 3NO_3^- + 98H^+ + 94e^- \tag{8}$$
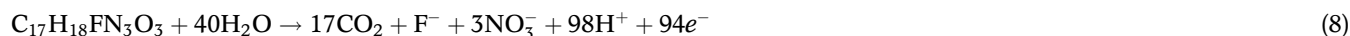
Since the wastewater treatment employed here uses electricity, it is necessary to compute the energy consumption (EC) because it is a very important economic parameter, which was estimated by using the following equation (Brillas *et al.* 2009),

$$EC\left(\frac{kWh}{gTOC}\right) = \frac{E_{Cell} \times i \times t}{V_s \times \Delta(TOC)_{Exp}} \tag{9}$$

where E_{cell} is the average cell voltage (V).

2.3.4. HPLC and mass spectrometry

The CIP degradation progress was conducted by using reverse-phase high-performance liquid chromatography (RP-HPLC) equipped with a photodiode detector (Agilent 6410). The column used was a Hypersil GOLD, 5 μm, 150 × 4.6 mm, the mobile phase was methanol grade HPLC and an aqueous solution of 0.1% formic acid. The isocratic separation was performed at 60/40 (v/v) with a flow rate of 1 mL min^{-1}. The sample was concentrated for Sep-Pak® C18 Cartridge (water-methanol), the injection volume on HPLC was of 15 μL and a temperature of 30 °C was used. To identify the CIP degradation compounds, a triple Quad LC/MS with an electrospray ionization (ESI) source was used. The mass spectrometry (MS) was carried out in positive ion mode, the capillary voltage at 3,000 V, nitrogen gas flow rate at 10 L min^{-1} and the gas temperature was 350 °C.

2.4. Experimental design of CIP electrolysis

2.5 L of synthetic wastewater of CIP (prepared with different CIP initial concentrations according to experimental design) was prepared and recirculated through the experimental set-up by means of a pump at a volumetric flow rate of 1 L min^{-1} to homogenize the solution in each run.

The factors studied in this research were pH_0, i, and $[C]_0$. All runs were performed by duplicate and the presented results correspond to the mean. The low, medium, and high levels are encoded as -1, 0, and $+1$, respectively, by using the following equation as shown in Table 2.

$$X_i = \frac{x_i - x_{i,0}}{\Delta x_i} \tag{10}$$

Table 2 | Levels and values of operational factors at a volumetric flow rate of 1 L min^{-1}

Factor	Level		
	−1	0	+1
X_1: pH$_0$	4.5	6.5	8.5
X_2: i (A)	3.0	3.5	4.0
X_3: $[C]_0$ (mg L^{-1})	10.0	30.0	50.0

For this optimization section, the removal efficiency of CIP was measured by UV-Vis spectrophotometric technique. For this purpose, the initial and final (within 5 h treatment) concentration ($[C]$) were measured for operating conditions according to Table 2. The experimental design was designed by a response surface methodology (RSM) employing a central composite face-centered design (CCFCD). The total experimental runs were 13 which are shown in Table 3. They were designed as follows: 2^{k-1} factorial points, $2k$ axial points, and k central points, with $k = 3$ and two responses (removal efficiency (η) and operating cost ($OCost$)).

Three additional experiments were performed at optimal operating conditions to validate the optimal operating conditions found and obtain the kinetic degradation of CIP, pathway reaction rate, EC, the MCE, and the mineralization grade (φ).

2.5. Optimization process

To accomplish this stage, the RSM designed above was employed to perform an analysis of the influence of the factors pH$_0$, i, and $[C]_0$ and their interactions, pH$_0 \times i$, pH$_0 \times [C]_0$, and $i \times [C]_0$, on responses (η (%) and $OCost$ ($MXN)) and to establish the optimal operating conditions. Upon performing the 13 runs, a quadratic (Equation (11)) and linear model (Equation (12)) for η (%) and $OCost$ were fitted, respectively, in order to describe the removal efficiency of CIP and compute the optimal operating conditions of the electrochemical degradation treatment of CIP.

$$\eta(\%) = \beta_0 + \sum_{i=1}^{k} \beta_i X_i + \sum_{i=1}^{k} \beta_{ii} X_i^2 + \sum_{i=1}^{k} \sum_{j=i+1}^{k} \beta_{ij} X_i X_j + \varepsilon \qquad (11)$$

$$OCost = \beta_0 + \sum_{i=1}^{k} \beta_i X_i + \varepsilon \qquad (12)$$

Table 3 | CCFCD for removal efficiency of CIP at a volumetric flow rate of 1 L min^{-1}

Run	Space type	Factor			Response	
		pH$_0$	i (A)	$[C]_0$ (mg L^{-1})	η (%)	$OCost$ ($MXN)
1	Factorial	8.5	4.0	10	95.261	1.048
2	Center	6.5	3.5	30	96.651	0.839
3	Axial	6.5	3.5	50	93.459	0.852
4	Factorial	4.5	3.0	10	96.435	0.663
5	Center	6.5	3.5	30	96.387	0.841
6	Axial	6.5	3.5	10	95.776	0.858
7	Axial	8.5	3.5	30	97.363	0.846
8	Axial	6.5	4.0	30	96.573	1.053
9	Axial	6.5	3.0	30	96.565	0.656
10	Factorial	4.5	4.0	50	96.730	1.044
11	Factorial	8.5	3.0	50	93.612	0.652
12	Axial	4.5	3.5	30	97.678	0.860
13	Center	6.5	3.5	30	96.517	0.863

where β values are the regression coefficients, ε is the random error, and X_i and X_j are the encoded independent variables (given by Equation (10)). To evaluate the reliability and significance of the fitted polynomial functions analysis of variance (ANOVA) must be performed (Regalado-Méndez *et al.* 2020). It is worth mentioning that all plots and data analysis were carried out in Design Expert V 10.0 software package.

Finally, the accuracy precision of the fitted models was determined by the root mean square error index (RMSE) according to the following equation (Viana *et al.* 2018),

$$\text{RMSE} = \sqrt{\frac{1}{\ell}\sum_{i}^{\ell}(\eta_{i,\text{ pred}} - \eta_{i,\text{ exp}})^2} \tag{13}$$

where $\eta_{i,\text{ pred}}$ and $\eta_{i,\text{ exp}}$ are the predicted and experimental values for the responses, respectively, and ℓ is the total number of experiments.

3. RESULTS AND DISCUSSION

3.1. Model fitting

Based on all experimental data given by the set of runs in Table 3, two mathematical models for the removal efficiency of CIP and total operating cost were fitted, which are represented by the following equations, respectively,

Uncoded variables
$$\eta(\%) = 92.873 + 0.102pH_0 + 2.591i - 0.005[C]_0 - 0.82pH_0 \times i - \cdots$$
$$0.012pH_0 \times [C]_0 + 0.9515i \times [C]_0 + 0.234pH_0^2 - 0.004[C]_0^2$$
Coded variables
$$\eta(\%) = 96.551 - 0.1575X_1 + 0.004X_2 - 1.1585X_3 - 0.82X_1X_2 - \cdots$$
$$0.482X_1X_3 + 0.9155X_2X_3 + 0.9385X_1^2 - 1.9645X_3^2 \tag{14}$$

Uncoded variables
$$OCost(\$MXN) = -0.55011 - 0.00175pH_0 + 0.39i - 0.000175[C]_0$$
Coded variables
$$OCost(\$MXN) = 0.8519 - 0.0035X_1 + 0.1957X_2 - 0.0035X_3 \tag{15}$$

3.2. Influence between the factors

The negative signs of β values in Equations (14) and (15) in terms of coded variables indicate a negative effect on responses in contrast to positive signs of β values (Zhou *et al.* 2020). From Equation (14), η (%) increases when increases i (X_2) but decreases with pH_0 (X_1) and $[C]_0$ (X_3). Also, the interaction between i and $[C]_0$ (X_2X_3) has a favorable effect on η (%), while the interaction between pH_0 and i (X_1X_2) and pH_0 and $[C]_0$ (X_1X_3) has a negative effect on η (%). Additionally, in Equation (15), the negative sign of β values indicates a negative effect on *OCost* and in a similar way, the positive sign of β values indicates a positive effect on *OCost*.

3.3. Analysis of variance

ANOVA analysis for both selected responses (η and *OCost*) is shown in Table 4. ANOVA results show that both models fitted (quadratic (Equation (14)) and linear (Equation (15))) are significant since the *F*-values (224.319 and 1,364.81 for η and *OCost*, respectively) are greater than *P*-values (<0.0001 and <0.0001) for both responses (η and *OCost*, respectively) and that *P*-values are lower than 0.005 for both responses (η and *OCost*, respectively) according to reference (Dixit & Yadav 2019). Also, the lack of fit is not significant for both responses (η and *OCost*) because the *F*-values (0.2423 and 0.1213 for η and *OCost*, respectively) are lower than *P*-values (0.801 and 0.9855) and that *P*-values are greater than 0.005 for both responses (η and *OCost*, respectively), which implies that there is a significant correlation between the chosen responses (η and *OCost*) and the chosen variables (X_1, X_2 y X_3). Also, determination coefficients (R^2) were 0.9977 and 0.9978 for η and *OCost*, respectively, implying that the fitted models have high reproducibility of experimental

Table 4 | ANOVA for responses η (%) and *OCost* ($MXN)

Source	Sum of square	Degree of freedom	Mean square	F-value	P-value	Remark
Removal efficiency, η (%)						
Model	19.5180	8	2.4397	224.319	<0.0001	Significant
X_1	0.0496	1	0.0496	4.5615	0.0995	
X_2	0.000032	1	0.000032	0.0029	0.9593	
X_3	2.6842	1	2.6842	246.7987	<0.0001	
X_1X_2	0.8965	1	0.8965	82.4303	0.0008	
X_1X_3	0.3097	1	0.3097	28.4808	0.0059	
X_2X_3	1.1175	1	1.1175	102.7486	0.0005	
X_1^2	2.4326	1	2.4326	223.6650	0.0001	
X_3^2	10.6589	1	10.6589	980.0169	<0.0001	
Residual	0.0435	4	0.0108			
Lack of fit	0.0086	2	0.0043	0.2483	0.8010	Not significant
Pure error	0.0349	2	0.0174			
Cor error	19.5615	12				
$R^2 = 0.9977$; $R_{adj}^2 = 0.9933$; $R_{Pred}^2 = 0.9637$; Adequate precision = 48.6206; C.V. = 0.11%						
Operating cost, *OCost* ($MXN)						
Model	0.2298	3	0.0766	1364.81	<0.0001	Significant
X_1	0.0000735	1	0.0000735	1.3092	0.2820	
X_2	0.2297	1	0.2297	4,091.8115	<0.0001	
X_3	0.0000735	1	0.0000735	1.3092	0.2820	
Residual	0.0005	9	0.0000561			
Lack of fit	0.0001	7	0.0000215	0.1213	0.9855	Not significant
Pure error	0.0003	2	0.0001			
Cor error	0.2303	12				
$R^2 = 0.9978$; $R_{adj}^2 = 0.9970$; $R_{Pred}^2 = 0.9968$; Adequate precision = 95.8414; C. V. = 0.88%						

data for both responses (η and *OCost*) (Korde *et al.* 2021). Moreover, the difference between R_{Adj}^2 and R_{Pred}^2 were 0.0296 and 0.0002 for η and *OCost*, respectively. The RMSE index performances were 0.2788 and 0.0062 for η and *OCost*, respectively, indicating that the fitted models (Equations (14) and (15)) have high concordance between predicted and experimental data. Furthermore, the adequate precession ratios for both responses were 48.62 and 95.84 for η and *OCost*, respectively, indicating an adequate signal since are greater than 4, according to reference (Peralta-Reyes *et al.* 2022) and the coefficient of variance was 0.1085 and 0.8794% for η and *OCost*, respectively, which indicates that the fitted models have high reproducibility since the C.V. was less than 10% for both responses (η and *OCost*). Hence, the models can be used to navigate the design space and are suitable for finding the optimal operating conditions of the electrochemical process employed.

Parity plots are displayed in Figure 2, which show that there are exceptionally good correlations between experimental data and predicted data by fitted models (Equations (14) and (15)) for both chosen responses (η and *OCost*).

Perturbation diagrams (Figure 3(a) and 3(b)) reveal that the most important factor for response η is the initial concentration of CIP ($[C]_0$ (X_3)) following the initial hydrogen potential (pH$_0$ (X_1)) since it presents a pronounced curvature. Also, the less important factor is the current intensity (i (X_2)) because has a relatively small slope. While for response *OCost*, the most important factor is the current intensity (i (X_2)) because of their high slope. Also, the less important factors were $[C]_0$ (X_3) and pH$_0$ (X_1) since their slopes are practically null.
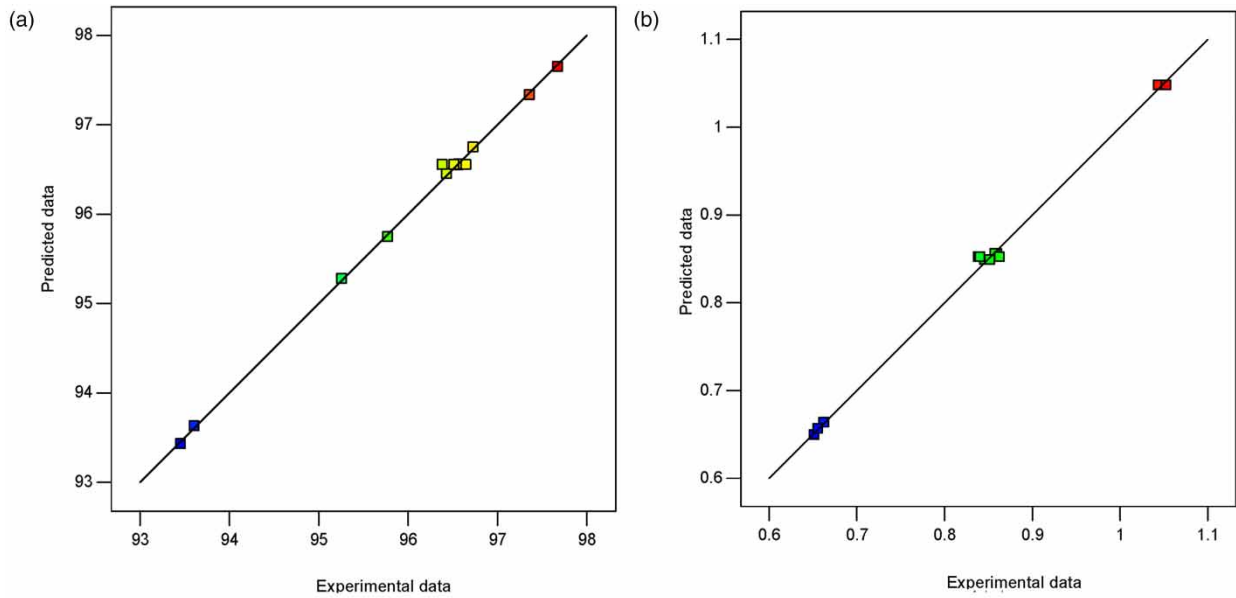
Figure 2 | Experimental data versus predicted values. (a) Response η; (b) Response *OCost*.
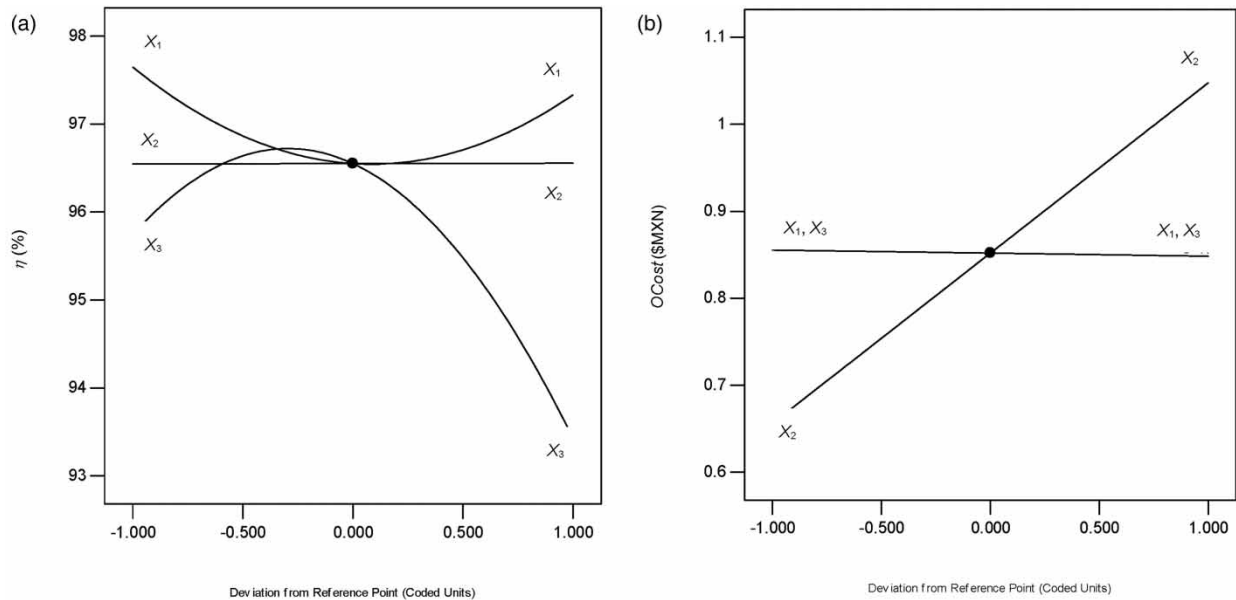

Figure 3 | Perturbation diagrams. (a) Response η and (b) Response *OCost*.

3.4. Optimization of the responses (η and *OCost*)

To optimize the chosen responses (η (Equation (14) and *OCost* (Equation (15))), a multi-objective optimization was performed by using the Design Expert V.10 software package. Additional information to be supplied in the software, such as the optimization criteria are shown in Table 5 in which all factors (X_1, X_2, and X_3) and both responses (η *and OCost*) have the same importance ($+++$).

The surface response plots are depicted in Figure 4(a)–4(f), which can be obtained by plotting Equations (14) and (15), respectively. In these 3D plots, the influence of pH_0, i, and $[C]_0$ on both responses (η and *OCost*) can be observed, maintaining constant one independent variable and varying the other two independent variables between study intervals.

Table 5 | Restrictions and optimization criteria for the electrochemical degradation of CIP

Response	Objective	Limits		Unit	Importance
		Min	Max		
pH_0	Is in range	4.50	8.50	Dimensionless	$+++$
i	Is in range	3.00	4.00	A	$+++$
$[C]_0$	Is in range	10.00	50.0	mg L^{-1}	$+++$
η	Maximize	93.46	97.68	%	$+++$
$OCost$	Minimize	0.65	1.05	\$MXN	$+++$

Figure 4(a)–4(c) forms a 3D plane since contour plots are shaped by linear functions. Changes in pH_0 and $[C]_0$ do not have a significant effect on $OCost$ but an increase in i has a negative effect on $OCost$ because the $OCost$ must be minimized.

Figure 4(d)–4(f) forms a saddle point since the contour plots are shaped by hyperboles. Also, an increase in pH_0 has a positive effect on η (see Figure 4(d) and 4(f)). An increase in $[C]_0$ has a negative effect on η (see Figure 4(e) and 4(f)). An increase in i has a positive effect on η in Figure 4(d) but a negative effect on η in Figure 4(e).

The maximum η (97.67%) and minimum $OCost$ (\$0.6521 MXN or 0.0354 US\$) were achieved at $pH_0 = 8.49$, $i = 3$ A, and $[C]_0 = 33.26$ mg L^{-1} within 5 h of electrolysis time with a global desirability of 99.97% indicating that all objectives were reached (see Figure 4h). Figure 4g depicts with black lines the restrictions (see Table 5) and a yellow section which represents the optimal operation region, which is bounded by a $pH_0 = 2.5$–9.5 and $i = 3$–4 A, and the gray section that represents the not feasible region.

3.5. Model verification

Three complementary runs were performed at optimal operating conditions to carry out the verification of the fitting models (Equations (14) and (15)). It is worth mentioning that the response η was followed by UV-Vis and HPLC. The average values for experimental response η were 94.17% by HPLC and 93.43% by UV-Vis, the error between these values was 0.78%, indicating that the use of the spectrophotometric UV-Vis technique is acceptable in this study for the optimization process. For complex effluents, however, the use of HPLC is advised. The computed percentage error for response η was 3.6 and 4.35% for HPLC and UV-Vis, respectively. Also, the $OCost$ was \$0.664 MXN (0.0325 US\$, 1 US\$/\$18.4238 MXN), with an error of 1.8%. Hence, the low (less than 5%) deviation between the values of experimental and modeled data corroborates the effectiveness of the optimization process employed in this work.

An additional trial at optimal operating conditions was carried out to show that the CIP is degraded with time (see Figure 5). Also, in Figure 5, the abatement of concentration of CIP is depicted.

Additionally, a TOC analysis at optimal operating conditions was carried out to analyze the fraction of TOC abatement as a function of time (see Figure 6(a)), MCE (%) as a function of time (see Figure 6(b)), and EC (kWh g^{-1} TOC) as a function of time (see Figure 6(c)).

It can be observed in Figure 6(a) that the maximum mineralization efficiency was 80% within 5 h of treatment according to Equation (8). These results indicate that there are some recalcitrant by-products and to achieve the total mineralization (CO_2, H_2O, and ions) a longer reaction time is required (Câmara Cardozo *et al.* 2022). Figure 6(b) shows a maximum of MCE at 5 h of electrolysis, indicating that CIP is transformed into byproducts easily degradable to transform into CO_2 due to hydroxyl radical produced following Equation (1) (Flox *et al.* 2007), which minimizes the parasitic reactions given by Equations (16)–(18) (Lanzarini-Lopes *et al.* 2017). Also, in Figure 6(c), a minimal value of EC (5.11 kWh g^{-1} TOC) is achieved at 5 h of treatment in agreement with the removed fraction of TOC (Brillas & Martínez-Huitle 2015). Furthermore, the maximum EC (23.25 kWh g^{-1} TOC) was at 1 h of electrolysis time.
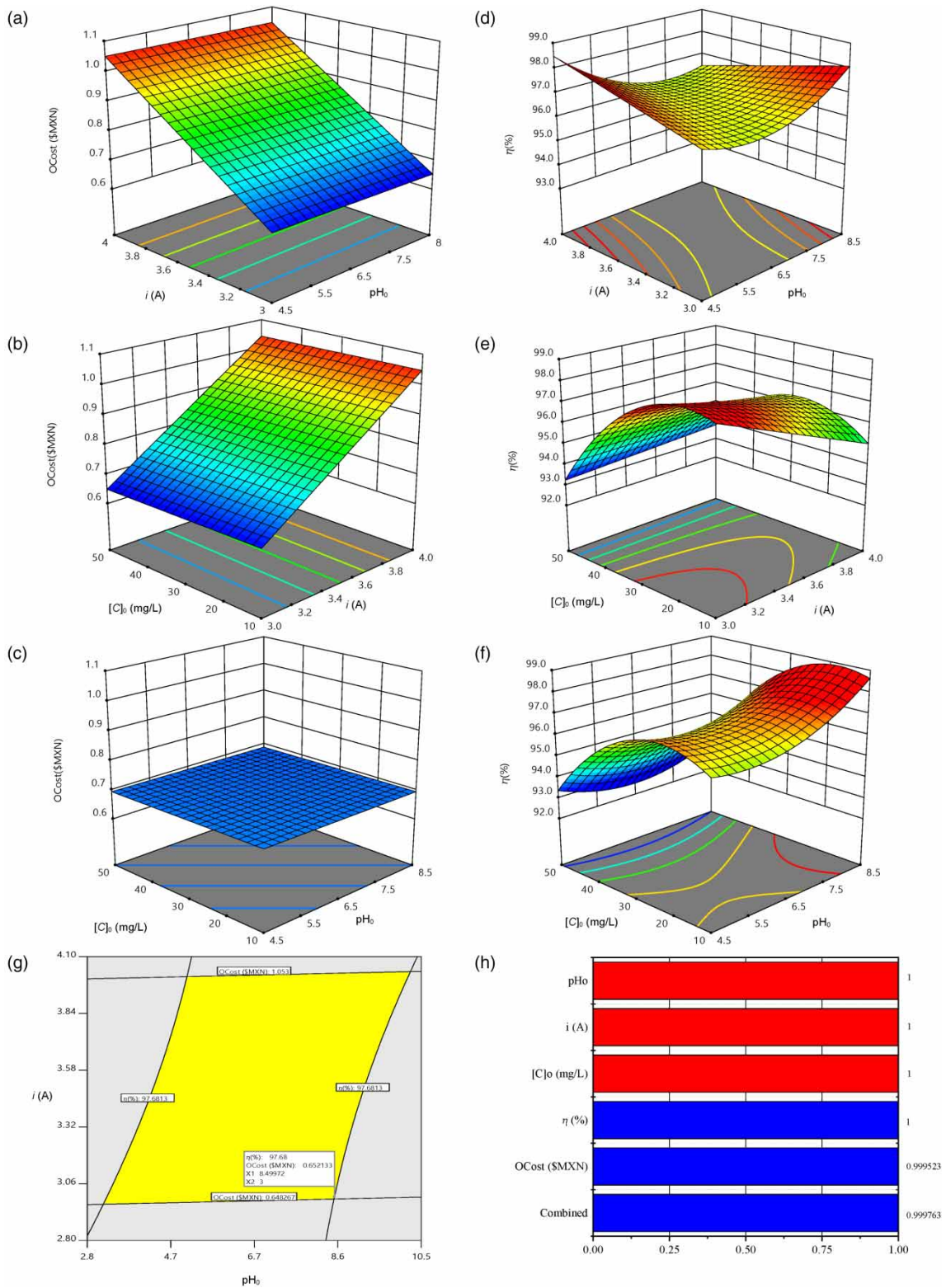
$$2H_2O^{\cdot} \rightarrow O_2 + 4H^+ + 4e^- \tag{16}$$

$$2OH^{\cdot} \rightarrow H_2O_2 \tag{17}$$

$$H_2O_2 + OH^{\cdot} \rightarrow HO_2^{\cdot} + H_2O \tag{18}$$

Figure 4 | (a) 3D plot of *OCost* as a function of pH$_0$ and *i*; (b) 3D plot of *OCost* as a function of *i* and [*C*]$_0$; (c) 3D plot of *OCost* as a function of pH$_0$ and [*C*]$_0$; (d) 3D plot of η as a function of pH$_0$ and *i*; (e) 3D plot of η as a function of *i* and [*C*]$_0$; (f) 3D plot of η as a function of pH$_0$ and [*C*]$_0$; (g) Overlay plot as a function of pH$_0$ and *i*; (h) Desirability bar chart. Please refer to the online version of this paper to see this figure in colour: https://dx.doi.org/10.2166/wst.2023.279.
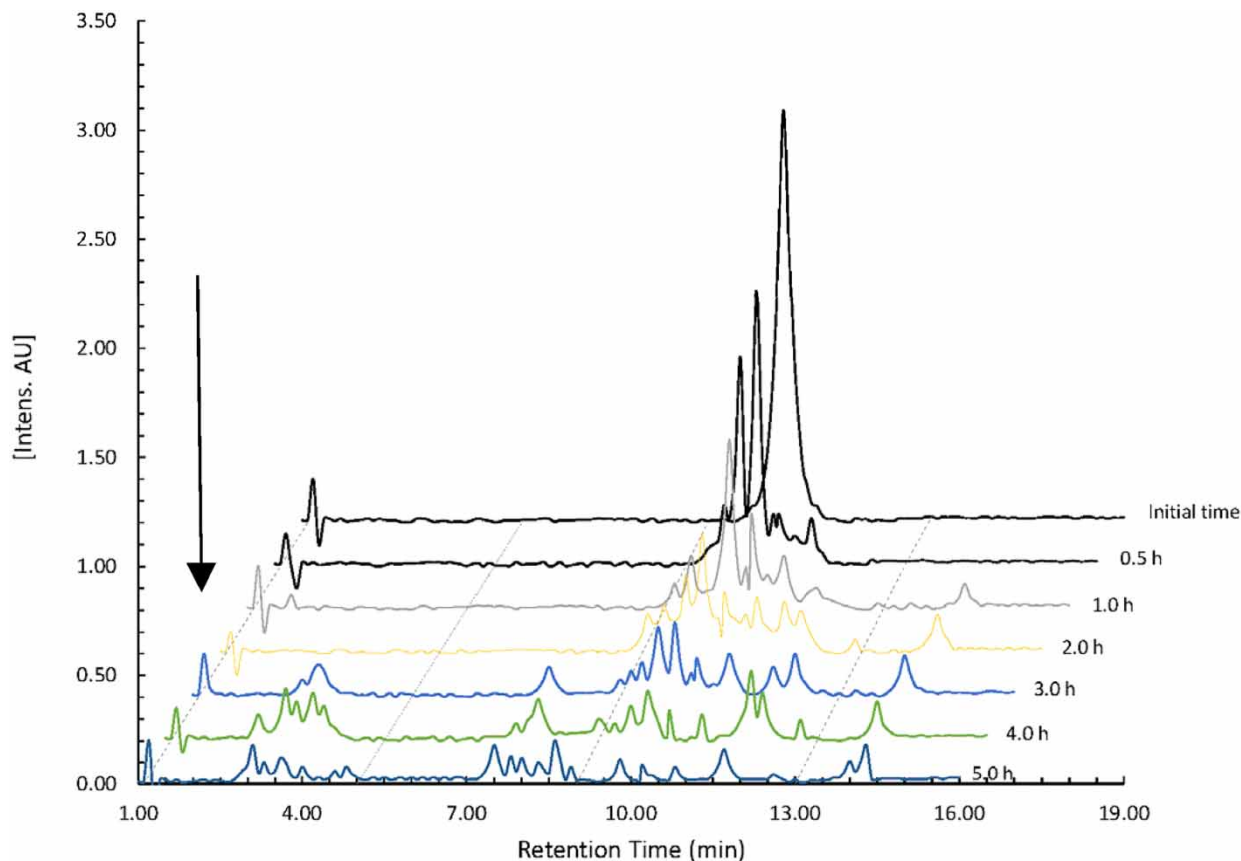
Figure 5 | Abatement of concentration of CIP as a function of time by HPLC at optimal operating conditions ($pH_0 = 8.49$, $i = 3$ A and $[C]_0 = 33.26$ mg L^{-1}, and $Q = 1$ L min^{-1}).

To understand if the electrochemical process employed in this research is controlled by mass transport or current, the limit current density (j_{lim}) must be computed by using the following equations (Chang *et al.* 2017),

$$\text{Ln}\left(\frac{\text{TOC}_t}{\text{TOC}_0}\right) = -\underbrace{\frac{A}{V_s}k_m}_{\text{slope}} t \tag{19}$$

$$j_{\text{lim}} = nFk_m[C]_0 \tag{20}$$

where n is the number of electrons, F is the Faraday constant, k_m average mass transfer coefficient, $[C]_0$ is the initial concentration of CIP, TOC_t is the TOC at any time t, TOC_0 is the initial TOC, V_s is the volume treatment, and A is the geometric area of the electrode.

For this case of study, the $j_{\text{lim}} = 3.09 \times 10^{-3}$ A cm^{-2}, $j_{\text{apply}} = 9.37 \times 10^{-2}$ A cm^{-2}, and $k_m = 7.04 \times 10^{-5}$ m s^{-1} were found. Hence, since the $j_{\text{apply}} > j_{\text{lim}}$ the electrochemical process is controlled by mass transport according to reference (Kapałka *et al.* 2008).

Finally, the extent of electrochemical combustion (φ) of the removed CIP was estimated as the ratio of the percentage TOC removed and the percentage CIP removed, according to Equation (21) (Miwa *et al.* 2006) in order to find the level of total combustion/removal. If φ tends towards 1, then almost all the CIP removed is subsequently mineralized into CO_2.

$$\varphi = \frac{\%\text{TOC}_{\text{removed}}}{\%\text{CIP}_{\text{removed}}} \tag{21}$$

where $\%\text{TOC}_{\text{removed}}$ is the percentage of TOC removed and $\%\text{CIP}_{\text{removed}}$ is the percentage of CIP removed.
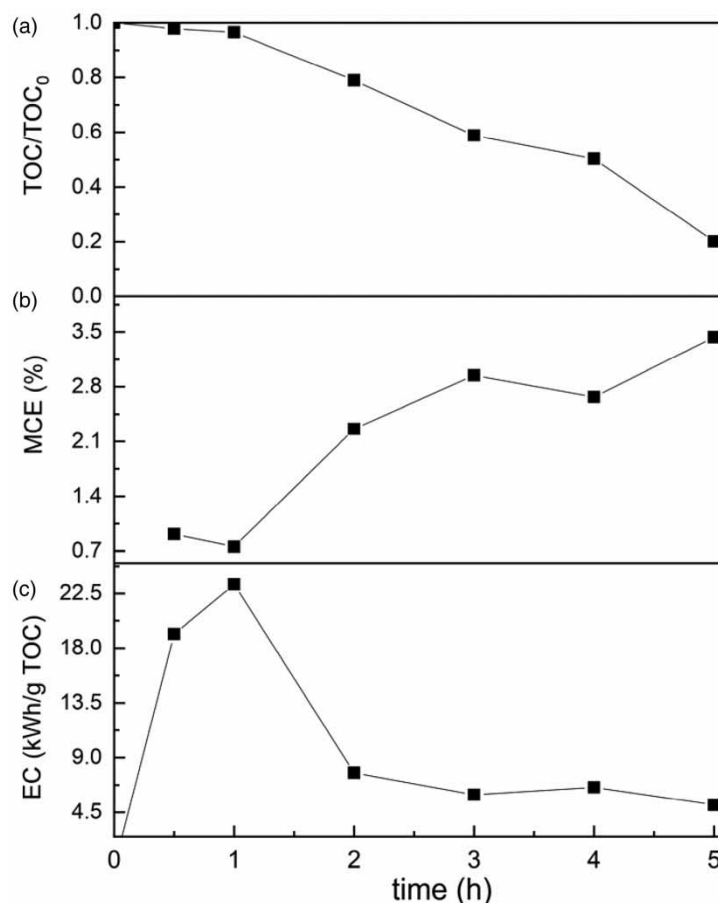
Figure 6 | TOC analysis of CIP at optimal operating conditions ($pH_0 = 8.49$, $i = 3$ A and $[C]_0 = 33.26$ mg L^{-1}, and $Q = 1$ L min^{-1}). (a) Fraction of TOC abatement; (b) MCE (%); (c) EC (kWh/g TOC).

The maximum value of φ was 0.85, indicating that the major amount of CIP was mineralized within 5 h of treatment time. These results corroborate the fact that BDD electrodes promote efficiently the complete oxidation of organic compounds such as CIP into CO_2. Also, the profile of φ is shown in Figure 7.

3.6. Degradation kinetics

Figure 8 depicts the electrochemical degradation of CIP followed by HPLC. An asymptotic behavior is observed, which is due to the intensive contact between CIP and OH$^\cdot$ generated in the electrode surface. Therefore, the CIP is relatively easily diffused on the BDD electrode surface and reacts with the OH$^\cdot$. Based on the behavior displayed in Figure 8, the electrochemical degradation of CIP follows a pseudo-first-order kinetic rate. From a linear regression analysis, the k_{app} value was 0.53 h^{-1} with a determination coefficient (R^2) value of 0.9921. Moreover, a good linear correlation ($R^2 > 0.9$) suggests a high amount of OH$^\cdot$ production on the BDD electrode surface (Sirés *et al.* 2008).

$$\ln\left(\frac{[C]_0}{[C]_t}\right) = \underbrace{k[\text{OH}^\cdot]}_{k_{app}} t \tag{22}$$

where k_{app} is the apparent kinetic reaction constant and t is the reaction time.

Finally, the kinetic order of the electrochemical mineralization of CIP was found by analyzing the TOC decay behavior depicted in Figure 6(a). After a linear regression analysis, it was found that the TOC removal fits a pseudo-zero-order kinetics rate, $-dTOC/dt = k_0$, where k_0 is the pseudo-zero-order rate constant ($k_0 = 3.3$ mg TOC L^{-1} min^{-1} with an R^2 value of 0.9566).
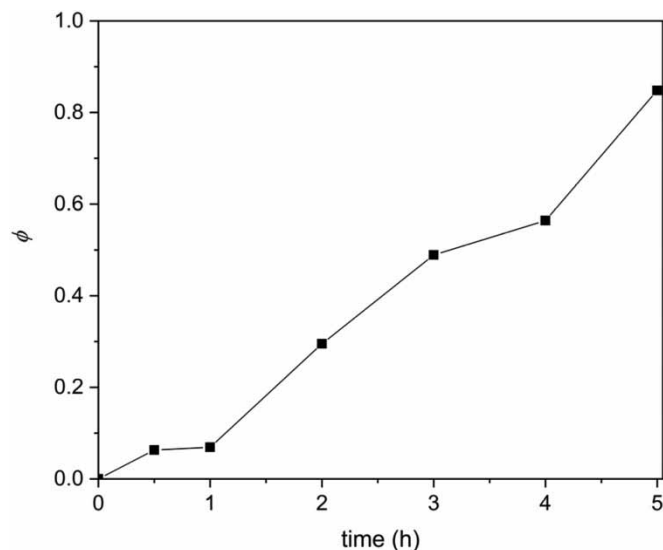
Figure 7 | Extent of electrochemical combustion (φ) of the removed CIP at optimal operating conditions (pH$_0$ = 8.49, i = 3 A and [C]$_0$ = 33.26 mg L^{-1}, Q = 1 L min^{-1}, and t = 5 h).

$$\frac{d[C_{CIP}]}{dt} = -0.53 h^{-1}[C_{CIP}]$$
$$R^2 = 0.9921$$

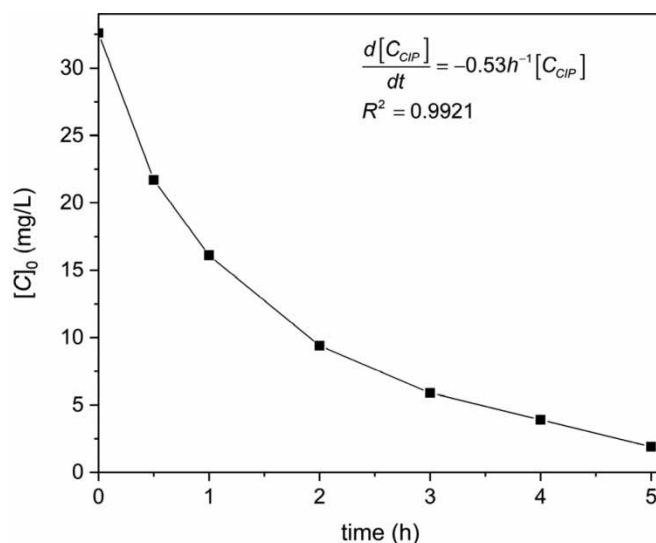**Figure 8** | Degradation profile of CIP at optimal operating conditions (pH$_0$ = 8.49, i = 3 A and [C]$_0$ = 33.26 mg L^{-1}, Q = 1 L min^{-1}, and t = 5 h).
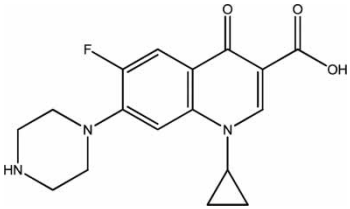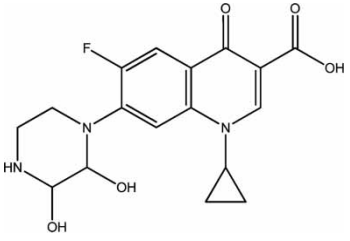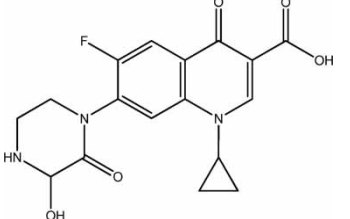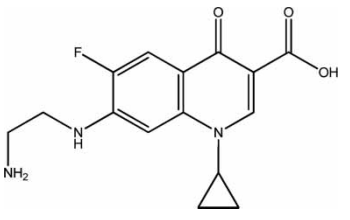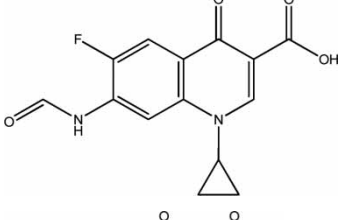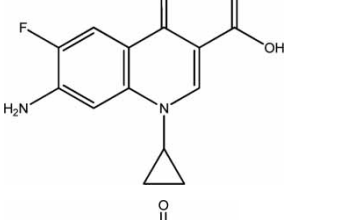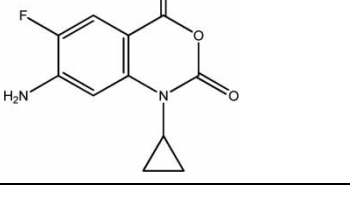
3.7. By-products identification

The identification of the by-products remaining after the electrochemical treatment at optimal operating conditions was performed by LC–MS. By this technique, 18 chemical organic structures were identified, and these are presented in Table 6. These chemical compounds were formed mainly by the attack of the OH$^{\cdot}$ on the rings of quinolone and cyclic diamines, which are the precursor molecules of CIP.

3.8. Reaction pathway

The fragmentation patterns obtained through ESI-MS analysis at different exposure times of ciprofloxacin to AOP revealed three possible degradation routes (see Figure 9 and Table 6). In the first one, a double hydroxylation was observed on the piperazine ring (m/z: 363.89), followed by the oxidation of an alcohol group and the formation of a carbonyl group on the same ring (m/z: 361.85). This led to the fragmentation of the piperazine ring, resulting in secondary and primary amines

Table 6 | Identified compounds after the electrochemical degradation of CIP at optimal operating conditions

Molecular formula	Chemical structure	Exact mass (m/z)	RT (min)	Degradation time (h)
$C_{17}H_{18}FN_3O_3$		331.64052	8.86	0.5
$C_{17}H_{18}FN_3O_5$		363.89234	9.86	1
$C_{17}H_{16}FN_3O_5$		361.85437	10.80	1, 2
$C_{15}H_{16}FN_3O_3$		305.79872	7.86	1, 2, 3
$C_{14}H_{11}FN_2O_4$		290.18696	10.39	2, 3, 4
$C_{13}H_{11}FN_2O_3$		263.07752	11.13	2, 3, 4
$C_{17}H_9FN_2O_3$		236.38752	12.80	3, 4

(*Continued.*)

Table 6 | Continued

Molecular formula	Chemical structure	Exact mass (m/z)	RT (min)	Degradation time (h)
$C_{17}H_{18}FN_3O_4$		347.66728	8.93	0.5, 1
$C_{17}H_{20}FN_3O_4$		349.40359	13.14	1, 2
$C_9H_{12}FN_3O$		197.52390	5.62	2, 3
$C_7H_6FN_2O$		153.17656	2.46	3, 4
$C_{14}H_{14}FN_3O_4$		307.59945	9.23	0.5, 1
$C_{14}H_{12}FN_3O_5$		321.28149	9.72	1, 2
$C_{11}H_{12}FN_3O_4$		269.99877	13.0	2, 3

(Continued.)

Table 6 | Continued

Molecular formula	Chemical structure	Exact mass (m/z)	RT (min)	Degradation time (h)
$C_6H_6FN_2$		125.97859	13.86	3, 4
C_6H_6FN		111.50865	6.56	3, 4
$C_6H_{10}FN_2$		134.67847	1,43	4
$C_7H_7FN_20$		138.96735	4.56	3, 4
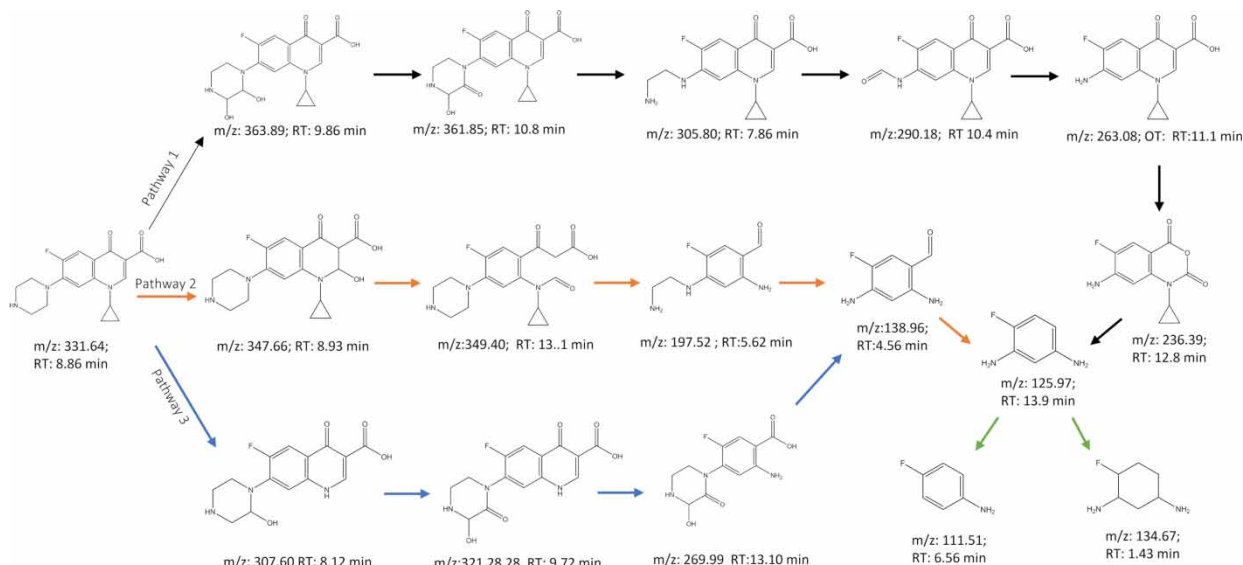
Figure 9 | Reaction pathway for electrochemical degradation of CIP with two BDD electrodes. Optimal reaction conditions: $pH_0 = 8.49$, $i = 3$ A, $[C]_0 = 33.26$ mg L^{-1}, and $Q = 1$ L min^{-1}.

(m/z: 305.80). Subsequently, the elimination of a primary amine formed a compound with m/z: 290.18. The last CO_2 molecule allowed the formation of the compound with m/z: 263.08. The compound with m/z: 263.08 underwent further degradation, involving the removal of a carboxyl (COOH) group and the hydropyridine ring. This resulted in the formation of an anhydrous group on the quinoline ring (m/z: 236.39). The carbonyl group facilitated the formation of inorganic CO_2, leading to the formation of a trisubstituted benzene ring (m/z: 125.97). The last two compounds identified at exposure times exceeding 5 h were aromatic compounds and cyclohexane (sp3), with masses of m/z: 111.51 and m/z: 134.67, respectively.

In the second pathway, the formation of a carbonyl group is the initial step for bond breakage, like the first pathway. The difference is the place where OH$^{\cdot}$ radicals attacked the ciprofloxacin ring. This pathway begins with the hydroxylation of the quinolone ring (m/z: 347.66), followed by the opening of the hydropyridine ring from the quinolone, identified as m/z: 349.40. Subsequently, the loss of the piperazine ring (m/z: 363.89) and the formation of an aldehyde group in the quinolone ring are necessary for the formation of m/z: 197.52. Completely, the molecule with m/z: 363.89 initially loses the piperazine ring, resulting in the formation of compounds with masses of m/z: 138.96 and m/z: 125.97, respectively. Both pathways converge in the formation of 4-fluoro-1,3-diaminobenzene (m/z: 125.97).

The third pathway begins with the loss of the cyclopropyl group and joins the hydroxylation of the piperazine ring m/z: 307.60, then the oxidation of the alcohol group forms the carbonyl group and there is another hydroxylation on the same piperazine ring, obtained the molecule m/z: 321.28. Subsequently, the degraded hydropyridine could be the origin of the molecule with m/z: 269.99. The analysis of the two pathways described above suggests that the degradation of the molecule with m/z: 269.99 could follow the loss of piperazine and quinoline, obtaining the formation of 4-fluoro-1,3-diaminobenzene (m/z: 125.97).

The description of the degradation path reveals that the action of the OH$^{\cdot}$ radical produces intermediates with carbonyl groups and smaller sizes, which facilitates the degradation of the molecules into CO_2 and H_2O consistent with previous results (Chen *et al.* 2021). In this research, three degradation routes are proposed in which the most susceptible groups are the piperazine and quinolone ring, as well as the cyclopropyl group, which coincides with what was reported in Van Doorslaer *et al.* (2014) and Chen *et al.* (2021). In relation to the determined molecules and other degradation routes, it is observed that the first pathway presents a similar behavior to those reported in anodic oxidations with graphite and silver electrodes at a concentration of 20 mg L^{-1} of CIP, a current density of 6.25 mA cm^{-2}, and a concentration of 0.1 mol L^{-1} of Na_2SO_4 (Chen *et al.* 2021). On the other hand, pathway two shows compounds like those reported in flow reactors with BDD electrodes at a current density of $j = 30$ mA cm^{-2}, pH = 10.0, a flow rate of 2.5 L min^{-1}, volume treated of 0.5 L, $[C_{CIP}] = 50$ mg L^{-1} in 0.1 M Na_2SO_4 (Wachter *et al.* 2019a). Finally, the third pathway is consistent with the results obtained in experiments with graphite and silver electrodes (Chen *et al.* 2021). It is important to mention that the by-products obtained are carbon compounds with fluorine atoms, which can be perfluoroalkyl pollutants (PFAS) that are frequently detected in water bodies. The stability of the carbon-fluorine bond hinders its degradation and favors its accumulation in plants and animals. The methods used (biotic and abiotic) for water purification do not degrade PFAS, which means that in industrialized societies a person can consume up to 70 ng of PFAS per liter of drinking water (Sunderland *et al.* 2019). Therefore, it is necessary to develop AOPs to achieve the complete degradation of the CIP.

It is also plausible that sulfate anions could affect the CIP oxidation by either scavenging hydroxyl radicals (Equation (23)) which may affect negatively the organic compounds oxidation (do Vale-Júnior *et al.* 2019)

$$2SO_4^- + 2OH^{\cdot} \rightarrow S_2O_8^{2-} + 2H_2O \tag{23}$$

Also, the sulfate radicals ($SO_4^{\cdot-}$) can be recombined with water to form hydroxyl radicals (Amado-Piña *et al.* 2017), as described by Equation (24). Therefore, this reaction is expected to favor the removal efficiency of the organic contaminant (e.g., CIP). It is worth mentioning, that this reaction only occurs when two BDD electrodes are employed.

$$SO_4^{\cdot-} + H_2O \rightarrow OH^{\cdot} \tag{24}$$

In this case, the scavenging of hydroxyl radicals is not expected to readily proceed since has been usually related to high amounts of sulfate ions (Duan *et al.* 2018; Ganiyu *et al.* 2021). Also, a series of other reactions could take place (Ganiyu *et al.* 2021) (Equations (25)–(30)). The amount of sulfate radical ($SO_4^{\cdot-}$) and persulfate ion ($S_2O_8^{2-}$) is also expected to increase when the electro-oxidation process is conducted at temperatures higher than 40 °C (Ganiyu & Martínez-Huitle 2019; Shin *et al.* 2019),

$$SO_4^{2-} + SO_4^{2-} \rightarrow S_2O_8^{2-} + 2e^- \tag{25}$$

$$SO_4^{\cdot-} + SO_4^{\cdot-} \rightarrow S_2O_8^{2-} \tag{26}$$

$$SO_4^- + e^- \rightarrow SO_4^{\cdot -} \tag{27}$$

$$SO_4^- + OH^{\cdot} \rightarrow SO_4^{\cdot -} + H^+ \tag{28}$$

$$S_2O_8^{2-} + e^- \rightarrow SO_4^{\cdot -} + SO_4^{2-} \tag{29}$$

$$S_2O_8^{2-} + \Delta \text{ ohmic heating} \rightarrow 2SO_4^{\cdot -} \tag{30}$$

In this study, the electrochemical oxidation of the CIP was carried out at a controlled temperature of 25 °C by using a heat exchanger. Thus, even if the previous reactions proceed, the impact on the CIP is expected to be low in comparison with the well-known production of hydroxyl radicals on BDD electrodes (Amado-Piña et al. 2022).

This agrees with those findings by Farhat et al. (2015), who mention that there is not enough evidence that activated persulfate species have a large effect on the removal efficiency of the organic compound when BDD anode is employed. Also, there is not enough evidence that high supporting electrolyte concentrations (Na_2SO_4, greater than 0.05 M) form high amounts of sulfate radicals and persulfate, when two BDD electrodes are employed. However, an excess of $SO_4^{\cdot -}$ could inhibit the removal efficiency of organic compounds through the self-quenching of $SO_4^{\cdot -}$ or the reaction between $SO_4^{\cdot -}$ and its maternal persulfate ion ($S_2O_8^{2-}$) molecule (see Equation (31)) when the concentration of persulfate is higher than the optimal concentration (Cai et al. 2018; Zhi et al. 2020).

$$SO_4^{\cdot -} + S_2O_8^{2-} \rightarrow SO_4^{2-} + S_2O_8^{2-\cdot} \tag{31}$$

A comparison of the different electrochemical degradation processes of CIP carried out in a flow reactor is shown in Table 7. In this table is distinguished that only this work reports the operating cost. Although the employed process achieves less degradation efficiency (94.17%) than all references given in Table 7 (100%) (Wachter et al. 2019a; dos Santos et al. 2022) the used volume in this research is 2.5–8.33 times greater than that employed in the literature. Albeit the mineralization efficiency achieved in reference (Wachter et al. 2019b) (100%) is greater than this research (80%), the volume used in this study is five times greater than that used in the literature. Given the results displayed in this work, the electrochemical treatment employed here could be considered adequate technology and profitable to be applied to wastewater that contains emerging contaminants such as CIP.

Table 7 | Comparison of the different electrochemical degradation processes of CIP in flow reactors

| Reaction environmental conditions | | | | Results | | | |
Optimized	Non optimized	Electrodes Cath-An	V (L)	ED (%)	TOC (%)	OCost (US$ L^{-1})	Ref.
$Q = 1$ L/min, pH$_0 = 8.49$, $i = 3$ A, $[C]_0 = 33.26$ mg L^{-1}, and $t = 5$ h		BDD-BDD	2.5	94.17	80	0.014	This work
	$Q = 2.5$ L min^{-1}, pH$_0 = 10$, $j = 30$ mA cm^{-2}, $[C]_0 = 50$ mg L^{-1}, $[Na_2SO_4] = 0.1$ mol L^{-1}, and $t = 10$ h	BDD-Stainless steel 304	0.5	100	100		Wachter et al. (2019a)
	$Q = 6.5$ L min^{-1}, pH$_0 = 10$, $j = 30$ mA cm^{-2}, $[C]_0 = 50$ mg L^{-1}, $[Na_2SO_4] = 0.1$ mol L^{-1}, and $t = 5$ h	Ni-TiPt/β-PBO$_2$-Ni BDD-Stainless steel 304	0.5	100	75		Wachter et al. (2019b)
	$Q = 7$ L min^{-1}, $j = 10$ mA cm^{-2}, $[C]_0 = 100$ mg L^{-1}, $[NaCl] = 0.1$ mol L^{-1}, and $t = 8$ h	BDD-Stainless steel 304	1.0	100	80		Carneiro et al. (2020)
	$Q = 0.4$ L min^{-1}, $j = 30$ mA cm^{-2}, pH$_0 = 7$, $[C]_0 = 10$ mg L^{-1}, and $t = 0.33$ h	BDD-Ti	0.3	100			Li et al. (2019)

4. CONCLUSIONS

CIP was degraded by an electro-oxidation process with BDD electrodes in a filter-press-type reactor. The optimal operating conditions were: $pH_0 = 8.49$, $i = 3$ A, $[C]_0 = 33.26$ mg L^{-1} at $Q = 1$ L min^{-1} within 5 h of electrolysis time.

The employed wastewater treatment in this research is an efficient and profitable technology because reaches high degradation efficiency (94.17%) and mineralization efficiency (80%) with a minimum operational cost (0.014 US$ L^{-1} or $MXN 0.2661 L^{-1}).

The optimization by RSM was successful in the electrochemical degradation of CIP because the differences between experimental data and predicted values from fitted models were 4.3 and 1.8% for η and *Ocost*, respectively.

The wastewater treatment proposed is environmentally friendly since there are not any solid residues produced and the EC is low (5.11 kWh g^{-1} TOC), which could be supplied easily by solar panels.

DATA AVAILABILITY STATEMENT

All relevant data are included in the paper or its Supplementary Information.

CONFLICT OF INTEREST

The authors declare there is no conflict.

REFERENCES

Ahmadzadeh, S., Asadipour, A., Pournamdari, M., Behnam, B., Rahimi, H. R. & Dolatabadi, M. 2017 Removal of ciprofloxacin from hospital wastewater using electrocoagulation technique by aluminum electrode: optimization and modelling through response surface methodology. *Process Safety and Environmental Protection* **109**, 538–547. Available from: https://www.sciencedirect.com/science/article/pii/S095758201730143X.

Amado-Piña, D., Roa-Morales, G., Barrera-Díaz, C., Balderas-Hernandez, P., Romero, R., Martín del Campo, E. & Natividad, R. 2017 Synergic effect of ozonation and electrochemical methods on oxidation and toxicity reduction: phenol degradation. *Fuel* **198**, 82–90. Available from: https://www.sciencedirect.com/science/article/pii/S0016236116310808.

Amado-Piña, D., Roa-Morales, G., Molina-Mendieta, M., Balderas-Hernández, P., Romero, R., Barrera Díaz, C. E. & Natividad, R. 2022 E-peroxone process of a chlorinated compound: oxidant species, degradation pathway and phytotoxicity. *Journal of Environmental Chemical Engineering* **10** (4), 108148. Available from: https://www.sciencedirect.com/science/article/pii/S2213343722010211.

Arman, N. Z., Salmiati, S., Aris, A., Salim, M. R., Nazifa, T. H., Muhamad, M. S. & Marpongahtun, M. 2021 A review on emerging pollutants in the water environment: existences, health effects and treatment processes. *Water (Switzerland)* **13** (22), 3258. https://doi.org/10.3390/w13223258.

Ashfaq, M., Khan, K. N., Rasool, S., Mustafa, G., Saif-Ur-Rehman, M., Nazar, M. F., Sun, Q. & Yu, C. P. 2016 Occurrence and ecological risk assessment of fluoroquinolone antibiotics in hospital waste of Lahore, Pakistan. *Environmental Toxicology and Pharmacology* **42**, 16–22.

Auguste, A. F. T. & Ouattara, L. 2021 Electrochemical degradation of amoxicillin on a $Ti/Ta_2O_5/Pt-RuO_2-IrO22$ electrode. *OALib* **8** (1), 1–13.

Barrera-Díaz, C. E., Frontana-Uribe, B. A., Rodríguez-Peña, M., Gomez-Palma, J. C. & Bilyeu, B. 2018 Integrated advanced oxidation process, ozonation-electrodegradation treatments, for nonylphenol removal in batch and continuous reactor. *Catalysis Today* **305**, 108–116. Available from: https://www.sciencedirect.com/science/article/pii/S0920586117306004.

Brillas, E. & Martínez-Huitle, C. A. 2015 Decontamination of wastewaters containing synthetic organic dyes by electrochemical methods. an updated review. *Applied Catalysis B: Environmental* **166–167**, 603–643. Available from: https://www.sciencedirect.com/science/article/pii/S0926337314007176.

Brillas, E., Sirés, I. & Oturan, M. A. 2009 Electro-Fenton process and related electrochemical technologies based on Fenton's reaction chemistry. *Chemical Reviews* **109** (12), 6570–6631. https://doi.org/10.1021/cr900136g.

Cai, J., Zhou, M., Yang, W., Pan, Y., Lu, X. & Serrano, K. G. 2018 Degradation and mechanism of 2,4-dichlorophenoxyacetic acid (2,4-D) by thermally activated persulfate oxidation. *Chemosphere* **212**, 784–793. Available from: https://www.sciencedirect.com/science/article/pii/S0045653518316023.

Câmara Cardozo, J., da Silva, D. R., Martínez-Huitle, C. A., Quiroz, M. A. & dos Santos, E. V. 2022 Photovoltaic electrochemically driven degradation of Calcon dye with simultaneous green hydrogen production. *Materials* **15** (21). Available from: https://www.mdpi.com/1996-1944/15/21/7445.

Cappelli, F., Longoni, O., Rigato, J., Rusconi, M., Sala, A., Fochi, I., Palumbo, M. T., Polesello, S., Roscioli, C., Salerno, F., Stefani, F., Bettinetti, R. & Valsecchi, S. 2022 Suspect screening of wastewaters to trace anti-COVID-19 drugs: potential adverse effects on aquatic environment. *Science of The Total Environment* **824**, 153756. Available from: https://www.sciencedirect.com/science/article/pii/S0048969722008488.

Carneiro, J. F., Aquino, J. M., Silva, B. F., Silva, A. J. & Rocha-Filho, R. C. 2020 Comparing the electrochemical degradation of the fluoroquinolone antibiotics norfloxacin and ciprofloxacin using distinct electrolytes and a BDD anode: evolution of main oxidation

byproducts and toxicity. *Journal of Environmental Chemical Engineering* **8** (6), 104433. Available from: https://www.sciencedirect.com/science/article/pii/S221334372030782X.

Chang, C.-F., Chen, T.-Y., Chin, C.-J. M. & Kuo, Y.-T. 2017 Enhanced electrochemical degradation of ibuprofen in aqueous solution by PtRu alloy catalyst. *Chemosphere* **175**, 76–84. Available from: https://www.sciencedirect.com/science/article/pii/S0045653517301996.

Chaplin, B. P. 2014 Critical review of electrochemical advanced oxidation processes for water treatment applications. *Environmental Sciences: Processes and Impacts* **16** (6), 1182–1203.

Chen, Z., Lai, W., Xu, Y., Xie, G., Hou, W., Zhanchang, P., Kuang, C. & Li, Y. 2021 Anodic oxidation of ciprofloxacin using different graphite felt anodes: kinetics and degradation pathways. *Journal of Hazardous Materials* **405**, 124262. Available from: https://www.sciencedirect.com/science/article/pii/S0304389420322524.

Dixit, S. & Yadav, V. L. 2019 Optimization of polyethylene/polypropylene/alkali modified wheat straw composites for packaging application using RSM. *Journal of Cleaner Production* **240**, 118228. Available from: https://www.sciencedirect.com/science/article/pii/S0959652619330987.

dos Santos, A. J., Fortunato, G. V., Kronka, M. S., Vernasqui, L. G., Ferreira, N. G. & Lanza, M. R. V. 2022 Electrochemical oxidation of ciprofloxacin in different aqueous matrices using synthesized boron-doped micro and nano-diamond anodes. *Environmental Research* **204**, 112027. Available from: https://www.sciencedirect.com/science/article/pii/S0013935121013220.

do Vale-Júnior, E., dos Santos, A. J., da Silva, D. R., Fajardo, A. S. & Martínez-Huitle, C. A. 2019 Electrochemical technologies for detecting and degrading benzoquinone using diamond films. *ChemElectroChem* **6** (17), 4383–4390. https://doi.org/10.1002/celc.201900541.

Duan, P., Hu, X., Ji, Z., Yang, X. & Sun, Z. 2018 Enhanced oxidation potential of Ti/SnO$_2$-Cu electrode for electrochemical degradation of low-concentration ceftazidime in aqueous solution: performance and degradation pathway. *Chemosphere* **212**, 594–603. Available from: https://www.sciencedirect.com/science/article/pii/S0045653518315984.

Esmaelian, M., Nabizadeh Chianeh, F. & Asghari, A. 2019 Degradation of ciprofloxacin using electrochemical oxidation by Ti/nanosno$_2$-MWCNT electrode: optimization and modelling through central composite design. *Journal of Industrial and Engineering Chemistry* **78**, 97–105. Available from: https://www.sciencedirect.com/science/article/pii/S1226086X18311882.

Farhat, A., Keller, J., Tait, S. & Adjenovic, J. 2015 Removal of persistent organic contaminants by electrochemically activated sulfate. *Environmental Science & Technology* **49** (24), 14326–14333. https://doi.org/10.1021/acs.est.5b02705.

Firdaus, I., Yaqub, A., Ajab, H., Khan, I., Ahmed, B., Amin, Z., Baig, A. & Isa, M. H. 2021 Electrochemical oxidation of amoxicillin, ciprofloxacin and erythromycin in water: effect of experimental factors on COD removal. *Pakistan Journal of Pharmaceutical Sciences* **34**, 119–128.

Flox, C., Cabot, P.-L., Centellas, F., Garrido, J. A., Rodríguez, R. M., Arias, C. & Brillas, E. 2007 Solar photoelectro-Fenton degradation of cresols using a flow reactor with a boron-doped diamond anode. *Applied Catalysis B: Environmental* **75** (1), 17–28. Available from: https://www.sciencedirect.com/science/article/pii/S0926337307000951.

Ganiyu, S. O. & Martínez-Huitle, C. A. 2019 Nature, mechanisms and reactivity of electrogenerated reactive species at thin-film boron-doped diamond (BDD) electrodes during electrochemical wastewater treatment. *ChemElectroChem* **6** (9), 2379–2392. https://doi.org/10.1002/celc.201900159.

Ganiyu, S. O., Martínez-Huitle, C. A. & Oturan, M. A. 2021 Electrochemical advanced oxidation processes for wastewater treatment: advances in formation and detection of reactive species and mechanisms. *Current Opinion in Electrochemistry* **27**, 100678. Available from: https://www.sciencedirect.com/science/article/pii/S2451910320302337.

Goswami, R. K., Agrawal, K. & Verma, P. 2022 An exploration of natural synergy using microalgae for the remediation of pharmaceuticals and xenobiotics in wastewater. *Algal Research* **64**, 102703.

Guinea, E., Arias, C., Cabot, P. L., Garrido, J. A., Rodríguez, R. M., Centellas, F. & Brillas, E. 2008 Mineralization of salicylic acid in acidic aqueous medium by electrochemical advanced oxidation processes using platinum and boron-doped diamond as anode and cathodically generated hydrogen peroxide. *Water Research* **42** (1), 499–511. Available from: https://www.sciencedirect.com/science/article/pii/S0043135407005222.

Kapałka, A., Fóti, G. & Comninellis, C. 2008 Kinetic modelling of the electrochemical mineralization of organic pollutants for wastewater treatment. *Journal of Applied Electrochemistry* **38** (1), 7–16. https://doi.org/10.1007/s10800-007-9365-6.

Khan, N. A., Khan, S. U., Ahmed, S., Farooqi, I. H., Yousefi, M., Mohammadi, A. A. & Changani, F. 2020 Recent trends in disposal and treatment technologies of emerging-pollutants- A critical review. *TrAC Trends in Analytical Chemistry* **122**, 115744. Available from: https://www.sciencedirect.com/science/article/pii/S0165993619305722.

Kim, T. K., Kim, T., Park, H., Lee, I., Jo, A., Choi, K. & Zoh, K. D. 2020 Degradation of ciprofloxacin and inactivation of ciprofloxacin resistant *E. faecium* during UV-LED (275 nm)/chlorine process. *Chemical Engineering Journal* **394**, 124803.

Korde, S., Deshmukh, S., Tandekar, S. & Jugade, R. 2021 Implementation of response surface methodology in physi-chemisorption of Indigo carmine dye using modified chitosan composite. *Carbohydrate Polymer Technologies and Applications* **2**, 100081. Available from: https://www.sciencedirect.com/science/article/pii/S2666893921000499.

Lanzarini-Lopes, M., Garcia-Segura, S., Hristovski, K. & Westerhoff, P. 2017 Electrical energy per order and current efficiency for electrochemical oxidation of p-chlorobenzoic acid with boron-doped diamond anode. *Chemosphere* **188**, 304–311. Available from: https://www.sciencedirect.com/science/article/pii/S004565351731384X.

Li, G., Zhou, S., Shi, Z., Meng, X., Li, L. & Liu, B. 2019 Electrochemical degradation of ciprofloxacin on BDD anode using a differential column batch reactor: mechanisms, kinetics and pathways. *Environmental Science and Pollution Research* **26** (17), 17740–17750.

Lima, V. B., Goulart, L. A., Rocha, R. S., Steter, J. R. & Lanza, M. R. V. 2020 Degradation of antibiotic ciprofloxacin by different AOP systems using electrochemically generated hydrogen peroxide. *Chemosphere* **247**.

Lupa, L., Cocheci, L., Trica, B., Coroaba, A. & Popa, A. 2020 Photodegradation of phenolic compounds from water in the presence of a Pd-Containing exhausted adsorbent. *Applied Sciences* **10** (23). Available from: https://www.mdpi.com/2076-3417/10/23/8440.

Martín de Vidales, M. J., Rua, J., de Juan, J. L. M., Fernández-Martínez, F. & dos Santos-García, A. J. 2020 Degradation of contaminants of emerging concern by electrochemical oxidation: coupling of ultraviolet and ultrasound radiations. *Materials* **13** (23), 1–12.

Miwa, D. W., Malpass, G. R. P., Machado, S. A. S. & Motheo, A. J. 2006 Electrochemical degradation of carbaryl on oxide electrodes. *Water Research* **40** (17), 3281–3289. Available from: https://www.sciencedirect.com/science/article/pii/S0043135406003988.

Montenegro-Ayo, R., Pérez, T., Lanza, M. R. V., Brillas, E., Garcia-Segura, S. & dos Santos, A. J. 2023 New electrochemical reactor design for emergent pollutants removal by electrochemical oxidation. *Electrochimica Acta* **458**, 142551. Available from: https://www.sciencedirect.com/science/article/pii/S0013468623007296.

Moreira, F. C., Boaventura, R. A. R., Brillas, E. & Vilar, V. J. P. 2017 Electrochemical advanced oxidation processes: a review on their application to synthetic and real wastewaters. *Applied Catalysis B: Environmental* **202**, 217–261.

Mu, Y., Huang, C., Li, H., Chen, L., Zhang, D. & Yang, Z. 2019 Electrochemical degradation of ciprofloxacin with a Sb-doped sno_2 electrode: performance, influencing factors and degradation pathways. *RSC Advances* **9** (51), 29796–29804.

Ojo, B. O., Arotiba, O. A. & Mabuba, N. 2022 Evaluation of $FTO-BaTiO_3/NiTiO_3$ electrode towards sonoelectrochemical degradation of emerging pharmaceutical contaminants in water. *Colloids and Surfaces A: Physicochemical and Engineering Aspects* **647**.

Peralta-Reyes, E., Vizarretea-Vásquez, D., Natividad, R., Aizpuru, A., Robles-Gómez, E., Alanis, C. & Regalado-Méndez, A. 2022 Electrochemical reforming of glycerol into hydrogen in a batch-stirred electrochemical tank reactor equipped with stainless steel electrodes: parametric optimization, total operating cost, and life cycle assessment. *Journal of Environmental Chemical Engineering* **10** (4), 108108. Available from: https://www.sciencedirect.com/science/article/pii/S2213343722009812.

Regalado-Méndez, A., Ruiz, M., Hernández-Servín, J. A., Natividad, R., Romero, R., Cordero, M. E., Estrada-Vázquez, C. & Peralta-Reyes, E. 2020 Electrochemical mineralization of ibuprofen on BDD electrodes in an electrochemical flow reactor: numerical optimization approach. *Processes* **8** (12), 1666.

Rivera-Utrilla, J., Sánchez-Polo, M., Ferro-García, M. Á., Prados-Joya, G. & Ocampo-Pérez, R. 2013 Pharmaceuticals as emerging contaminants and their removal from water. A review. *Chemosphere* **93** (7), 1268–1287.

Shin, Y.-U., Yoo, H.-Y., Ahn, Y.-Y., Kim, M. S., Lee, K., Yu, S., Lee, C., Cho, K., Kim, H. & Lee, J. 2019 Electrochemical oxidation of organics in sulfate solutions on boron-doped diamond electrode: multiple pathways for sulfate radical generation. *Applied Catalysis B: Environmental* **254**, 156–165. Available from: https://www.sciencedirect.com/science/article/pii/S0926337319303820.

Sirés, I., Brillas, E., Cerisola, G. & Panizza, M. 2008 Comparative depollution of mecoprop aqueous solutions by electrochemical incineration using BDD and PbO_2 as high oxidation power anodes. *Journal of Electroanalytical Chemistry* **613** (2), 151–159. Available from: https://www.sciencedirect.com/science/article/pii/S0022072807005049.

Sunderland, E. M., Hu, X. C., Dassuncao, C., Tokranov, A. K., Wagner, C. C. & Allen, J. G. 2019 A review of the pathways of human exposure to poly- and perfluoroalkyl substances (PFASs) and present understanding of health effects. *Journal of Exposure Science & Environmental Epidemiology* **29** (2), 131–147. https://doi.org/10.1038/s41370-018-0094-1.

Van Doorslaer, X., Dewulf, J., Van Langenhove, H. & Demeestere, K. 2014 Fluoroquinolone antibiotics: an emerging class of environmental micropollutants. *Science of the Total Environment* **500–501**, 250–269. Available from: https://www.sciencedirect.com/science/article/pii/S0048969714012546.

Viana, D. F., Salazar-Banda, G. R. & Leite, M. S. 2018 Electrochemical degradation of Reactive Black 5 with surface response and artificial neural networks optimization models. *Separation Science and Technology* **53** (16), 2647–2661. https://doi.org/10.1080/01496395.2018.1463264.

Wachter, N., Aquino, J. M., Denadai, M., Barreiro, J. C., Silva, A. J., Cass, Q. B., Bocchi, N. & Rocha-Filho, R. C. 2019a Electrochemical degradation of the antibiotic ciprofloxacin in a flow reactor using distinct BDD anodes: reaction kinetics, identification and toxicity of the degradation products. *Chemosphere* **234**, 461–470. Available from: https://www.sciencedirect.com/science/article/pii/S0045653519312913.

Wachter, N., Aquino, J. M., Denadai, M., Barreiro, J. C., Silva, A. J., Cass, Q. B., Rocha-Filho, R. C. & Bocchi, N. 2019b Optimization of the electrochemical degradation process of the antibiotic ciprofloxacin using a double-sided β-PbO_2 anode in a flow reactor: kinetics, identification of oxidation intermediates and toxicity evaluation. *Environmental Science and Pollution Research* **26** (5), 4438–4449. https://doi.org/10.1007/s11356-018-2349-8.

Wang, Y., Shen, C., Zhang, M., Zhang, B.-T. & Yu, Y.-G. 2016 The electrochemical degradation of ciprofloxacin using a SnO_2-Sb/Ti anode: influencing factors, reaction pathways and energy demand. *Chemical Engineering Journal* **296**, 79–89. Available from: https://www.sciencedirect.com/science/article/pii/S1385894716303461.

Zhi, D., Lin, Y., Jiang, L., Zhou, Y., Huang, A., Yang, J. & Luo, L. 2020 Remediation of persistent organic pollutants in aqueous systems by electrochemical activation of persulfates: a review. *Journal of Environmental Management* **260**, 110125. Available from: https://www.sciencedirect.com/science/article/pii/S0301479720300633.

Zhou, R., Zhang, M., Li, J. & Zhao, W. 2020 Optimization of preparation conditions for biochar derived from water hyacinth by using response surface methodology (RSM) and its application in Pb^{2+} removal. *Journal of Environmental Chemical Engineering* **8** (5), 104198. Available from: https://www.sciencedirect.com/science/article/pii/S2213343720305479.